Effective polarization in proton-induced α knockout reactions

Tomoatsu Edagawa [1,*] Kazuki Yoshida [2] Yoshiki Chazono [1,†] and Kazuyuki Ogata [1,3,‡]

[1]*Research Center for Nuclear Physics (RCNP), Osaka University, Ibaraki Osaka 567-0047 Japan*

[2]*Advanced Science Research Center, Japan Atomic Energy Agency (JAEA), Tokai, Ibaraki 319-1195, Japan*

[3]*Nambu Yoichiro Institute of Theoretical and Experimental Physics (NITEP), Osaka City University, Osaka 558-8585, Japan*

(Received 27 September 2022; accepted 13 April 2023; published 10 May 2023)

The effective polarization of the residual nucleus in the proton-induced α knockout reaction is investigated within the distorted wave impulse approximation framework. The strong absorption of the emitted α particle results in strong selectivity on the reaction position depending on the third component of the single-particle orbital angular momentum of the α particle inside a nucleus, hence on the spin direction of the reaction residue. This is caused by a mechanism that is similar to the Maris effect, the effective polarization in the proton-induced proton knockout reactions. However, as a distinct feature of the effective polarization in the α knockout process, the spin degrees of freedom of the reacting particles play no role. The α knockout process with complete kinematics can be a useful polarization technique for the residual nucleus, without actively controlling the spin of the proton.

DOI: 10.1103/PhysRevC.107.054603

I. INTRODUCTION

Proton-induced nucleon knockout reactions, (p, pN), have been developed to investigate the single-particle (s.p.) structure of nuclei [1,2]. In a recent review [3], the (p, pN) reactions were shown to be a reliable spectroscopic tool, meaning that the deduced spectroscopic factors are consistent with those determined by electron-induced knockout reaction data, typically within a deviation of 15%. In addition, the proton has the advantage of being able to knock neutrons out, whereas the electron can only strike charged particles. Then this has been opening a door to knockout reaction studies of neutron s.p. levels as well as s.p. structures of unstable nuclei. In recent years, a series of (p, pN) measurements has provided us with new findings on the s.p. structure and the magicity of unstable nuclei [4–19]. On the reaction theory side, the quantum transfer-to-the continuum model (QTC) [20,21], the eikonal DWIA [22], and the Faddeev–Alt-Grassberger-Sandhas theory (FAGS) [23–25] for knockout reactions have been developed; there are some benchmark type studies among them [26,27]. The knockout reactions have also been utilized as a probe of nuclear clustering. In Ref. [28], the first direct observation of α-particle formation on Sn isotopes, triggered by the theoretical prediction by Typel [29], was confirmed by the α knockout reaction.

It is shown that (p, pN) reactions mainly probe the surface region of nuclei because of the nuclear absorption [21,22,30]. Recently, by choosing the kinematics of the ^{11}Li(p, pn) process, the correspondence between the correlation angle of the two neutrons and their location inside ^{11}Li was investigated [13]; this work has triggered intensive discussion from a theoretical point of view [31,32]. Even though the nuclear distortion tends to prohibit a simple interpretation of the measured cross section, the result of Ref. [13] implies that, when light nuclei are considered, (p, pN) may probe the rather interior region of them because of the relatively weak nuclear absorption.

On the other hand, the surface sensitivity is expected to be more emphasized in proton-induced α knockout reactions, $(p, p\alpha)$ [33,34]. Furthermore, a clear selectivity in the reaction region of the ^{120}Sn$(p, p\alpha)$ was shown, meaning that only the α particle located on the near side of the target nucleus with respect to the direction of the emitted α is observed; see Fig. 8 of Ref. [33]. It should be noted that, as emphasized in Ref. [33], the selectivity not only in the radius but also in the direction of the target nucleus was suggested. We henceforth refer this to as the reaction position selectivity (RPS). It is noted that in Ref. [34], the radial selectivity of $(p, p\alpha)$ reaction is investigated. When the RPS is realized, one may also expect some selectivity in spin-dependent observables. In fact, the effective polarization [35–38], which is sometimes called the Maris effect, is a well-known phenomenon in (p, pN) reaction studies. A compact review of the Maris effect can be found in Sec. 2.3 of Ref. [3]. In short, the nucleons in a nucleus in the $j_> \equiv l + 1/2$ and $j_< \equiv l - 1/2$ s.p. orbits, where l is the nucleon orbital angular momentum ($l \neq 0$), are effectively polarized in opposite directions. It is argued that a rather strong spin correlation of nucleon-nucleon (NN) scattering at intermediate energies and the short mean-free path of an outgoing proton with low energy realize the RPS and hence the Maris effect.

The purpose of this study is to clarify the role of the RPS in $(p, p\alpha)$ reactions. Because α is a spinless particle, we do not have its effective polarization. Nevertheless, we can still

*tomoatsu@rcnp.osaka-u.ac.jp

†Present address: RIKEN Nishina Center for Accelerator-Based Science, 2-1 Hirosawa, Wako 351-0198, Japan.

‡Present address: Department of Physics, Kyushu University, Fukuoka 819-0395, Japan.

consider a polarization of the reaction residue, which is also the case with the nucleon knockout reaction. In this study, we consider the ^{120}Sn$(p, p\alpha)\,^{116}$Cd$_{2^+}$ and ^{20}Ne$(p, p\alpha)\,^{16}$O$_{2^+}$ reactions at 392 MeV and investigate how the reaction residue in the 2^+ excited state is polarized because of the RPS. In contrast to the previous research on the vector analyzing power of the $(p, p\alpha)$ reactions [39–43], a point in this work is that the unpolarized proton beam is considered and the effective polarization is not induced by any spin-dependent interactions.

It should be noted that in Ref. [44], spin alignment in one-nucleon removal reactions was discussed. The authors showed that the parallel momentum distribution of the ^{27}Mg$_{5/2^+}$ residue produced by removing a $d_{5/2}$ neutron from ^{28}Mg with a ^{9}Be target is dominated by the maximum magnetic quantum number components $m_l = \pm 2$. The mechanism of this spin alignment in Ref. [44] is similar to what we discuss below. However, in the present study, we aim at clarifying that just by considering kinematically complete measurement for α knockout reactions, without any help of the intrinsic spin of the particles involved, the spin polarization of the reaction residue can be achieved.

The construction of this paper is as follows. In Sec. II we describe the DWIA formalism for the $(p, p\alpha)$ reaction and the treatment of the reorientation of the quantization axis. We then show in Sec. III numerical results and how the residue of the $(p, p\alpha)$ reaction is effectively polarized. Finally, a summary is given in Sec. IV.

II. THEORETICAL FRAMEWORK

In the present study, the factorized form of the distorted wave impulse approximation (DWIA) without the spin degrees of freedom is employed. This framework has been recently applied to several studies on $(p, p\alpha)$ reactions [33,45–48]. The kinematics of the reaction is defined following the Madison convention [49]. The reduced transition matrix $\bar{T}$ within the DWIA framework [3,50,51] is given by

$$\bar{T}_m = \int d\boldsymbol{R}\, \chi^{(-)*}_{1,\boldsymbol{K}_1}(\boldsymbol{R})\chi^{(-)*}_{2,\boldsymbol{K}_2}(\boldsymbol{R})\chi^{(+)}_{0,\boldsymbol{K}_0}(\boldsymbol{R}) \times e^{-i\alpha_R \boldsymbol{K}_0\cdot\boldsymbol{R}}\psi_{nlm}(\boldsymbol{R}). \tag{1}$$

The incident, emitted protons, and emitted α are labeled as particles 0, 1, and 2, respectively, while the bound α in the initial state is labeled as b. The core nucleus in the initial state (the residue in the final state) is labeled as B in this paper. χ_i is a distorted wave of particle i (=0, 1, or 2) with its asymptotic momentum $\boldsymbol{K}_i$. The third component of an angular momentum corresponds to the z component unless otherwise noted. The outgoing and incoming boundary conditions of the distorted waves are denoted by superscripts $(+)$ and $(-)$, respectively. α_R is the mass ratio of the struck particle to the target, $4/120 = 1/30$ for ^{120}Sn$(p, p\alpha)\,^{116}$Cd$_{2^+}$ and $4/20 = 1/5$ for ^{20}Ne$(p, p\alpha)\,^{16}$O$_{2^+}$. n is the principal quantum number, and l and m, respectively, are the orbital angular momentum and its third component of b. Since α is a spinless particle, ψ^n_{lm} is written as

$$\psi_{nlm}(\boldsymbol{R}) = \varphi_{nl}(R)Y_{lm}(\hat{\boldsymbol{R}}), \tag{2}$$

where φ_{nl} is the radial part of the bound-state wave function and Y_{lm} is the spherical harmonics. In the present DWIA framework, the triple differential cross section (TDX) with respect to the proton emission energy $T^{\rm L}_1$, its emission angles $\Omega^{\rm L}_1$, and the α emission angle $\Omega^{\rm L}_2$ is given by

$$\frac{d^3\sigma^{\rm L}}{dT^{\rm L}_1 d\Omega^{\rm L}_1 d\Omega^{\rm L}_2} = \sum_{m_y}\left(\frac{d^3\sigma^{\rm L}}{dT^{\rm L}_1 d\Omega^{\rm L}_1 d\Omega^{\rm L}_2}\right)_{m_y}, \tag{3}$$

$$\left(\frac{d^3\sigma^{\rm L}}{dT^{\rm L}_1 d\Omega^{\rm L}_1 d\Omega^{\rm L}_2}\right)_{m_y} = F^{\rm L}_{\rm kin}\frac{E_1E_2E_{\rm B}}{E^{\rm L}_1E^{\rm L}_2E^{\rm L}_{\rm B}}\frac{(2\pi)^4}{\hbar v_\alpha}\frac{1}{2l+1} \times\frac{(2\pi\hbar^2)^2}{\mu_{p\alpha}}\frac{d\sigma_{p\alpha}}{d\Omega_{p\alpha}}\left|\bar{T}_{m_y}\right|^2. \tag{4}$$

Quantities with superscript L are evaluated in the laboratory frame while the others are in the center-of-mass frame of the three-body system. Here, $F^{\rm L}_{\rm kin}$ is the phase volume

$$F^{\rm L}_{\rm kin} = \frac{E^{\rm L}_1K^{\rm L}_1E^{\rm L}_2K^{\rm L}_2}{(\hbar c)^4}\left[1+\frac{E^{\rm L}_2}{E^{\rm L}_{\rm B}}+\frac{E^{\rm L}_2}{E^{\rm L}_{\rm B}}\frac{(\boldsymbol{K}^{\rm L}_1-\boldsymbol{K}^{\rm L}_0)\cdot\boldsymbol{K}^{\rm L}_2}{\left(K^{\rm L}_2\right)^2}\right]^{-1}, \tag{5}$$

and v_α, $\mu_{p\alpha}$, T_i, and E_i respectively, are the relative velocity of the incident proton and the target, reduced energy of p and α, the kinetic and the total energy of particle i (=0, 1, 2 or B). $d\sigma_{p\alpha}/d\Omega_{p\alpha}$ is the p-α elastic differential cross section in free space with p-α two-body scattering energy and angle determined by the $(p, p\alpha)$ kinematics. It should be noted that the TDX is decomposed into the components of each m_y, which is the projection of l on the y axis taken to be the direction of $\boldsymbol{K}_0 \times \boldsymbol{K}_1$. In other words, in the calculation of the TDX of Eqs. (3) and (4), the y axis is taken as the quantization axis. See Sec. 3.1 of Ref. [3] for details.

The transition matrix $\bar{T}_{m_y}$ in Eq. (4) can be obtained by reorientating the quantization axis of $\boldsymbol{l}$ from the z axis to the y axis,

$$\bar{T}_{m_y} = \sum_m D^l_{m_y,m}(\hat{\boldsymbol{R}}_{yz})\bar{T}_m, \tag{6}$$

where D is the Wigner's D-matrix and $\hat{\boldsymbol{R}}_{yz}$ is a rotation represented by Euler angles from the z axis to the y axis. The orthonormality and completeness of D ensure the invariance of the TDX under the reorientation of the quantization axis,

$$\sum_{m_y}\left|\bar{T}_{m_y}\right|^2 = \sum_m |\bar{T}_m|^2. \tag{7}$$

In the present study, $D^l_{m_y,m}$ in Eq. (6) only acts on the spherical harmonics Y_{lm} in Eq. (2) and reorientates its quantization axis.

III. RESULTS AND DISCUSSION

A. Numerical input

First, we consider the ^{120}Sn$(p, p\alpha)\,^{116}$Cd$_{2^+}$ cross section at 392 MeV. The recoilless condition, in which the momentum of the residue B in the final state is zero ($\boldsymbol{K}^{\rm L}_{\rm B} = 0$), is realized when $T^{\rm L}_1 = 328$ MeV, $\theta^{\rm L}_1 = 43.2^\circ$, $\phi^{\rm L}_1 = 0^\circ$, $\theta^{\rm L}_2 = 61^\circ$, and $\phi^{\rm L}_2 = 180^\circ$. These conditions are determined by an available

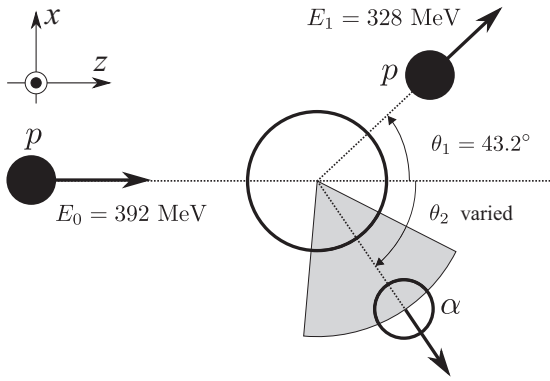

FIG. 1. The kinematical setup of the ^{120}Sn$(p, p\alpha)\,^{116}$Cd$_{2+}$ reaction.

setup at RCNP, expecting such experiments will be conducted in the near future. The TDX$_{m_y}$ around the recoilless condition is calculated by varying $\theta_2^{\rm L}$. The kinematical setup is shown in Fig. 1.

The α cluster wave function ψ_{nlm} is obtained as a bound state of α and ^{116}Cd within a Woods-Saxon potential,

$$V(R) = \frac{V_0}{1 + \exp\left(\frac{R-R_0}{a}\right)}. \tag{8}$$

Its range and diffuseness parameters are $R_0 = 1.27 \times 116^{1/3}$ fm and $a = 0.67$ fm, respectively. The depth parameter V_0 is determined to reproduce the α separation energy of ^{120}Sn. We consider $n = 7$ and $l = 2$, and ψ_{nlm} is normalized to unity; n is determined by the orthogonality condition model [52]. The p-α differential cross section in free space in Eq. (4) is obtained by the microscopic single-folding model [53] with a phenomenological α density in free space and the Melbourne nucleon-nucleon g-matrix interaction [54]. For the α density, we use the phenomenological proton density [55] determined from electron scattering in which the finite-size effect due to the proton charge is unfolded in the standard manner [56]. The neutron density is assumed to have the same geometry as the proton one. The p-^{120}Sn and p-^{116}Cd distorted waves are obtained as a scattering state under the Koning-Delaroche global optical potential [57]. As for the α-^{116}Cd distorted wave, the global α optical potential proposed by Avrigeanu *et al.* [58] is adopted. For comparison, we also use microscopic optical potentials. The p-^{120}Sn, p-^{116}Cd, and n-^{116}Cd potentials are obtained by the single-folding model with the Melbourne g matrix and nuclear densities of ^{120}Sn and ^{116}Cd calculated with the Bohr-Mottelson s.p. potential [59]. The α-^{116}Cd potential is obtained by the nucleon-nucleus folding (NAF) model [60] with the p-^{116}Cd and n-^{116}Cd potentials.

B. Effective polarization in $(p, p\alpha)$ reaction

We show in Fig. 2 the TDX$_{m_y}$ as a function of $p_{\rm R}$:

$$p_{\rm R} = \hbar K_{\rm B}^{\rm L} \frac{K_{{\rm B}z}^{\rm L}}{|K_{{\rm B}z}^{\rm L}|}, \tag{9}$$

with $K_{{\rm B}z}^{\rm L}$ being the z component of $\boldsymbol{K}_{\rm B}^{\rm L}$.

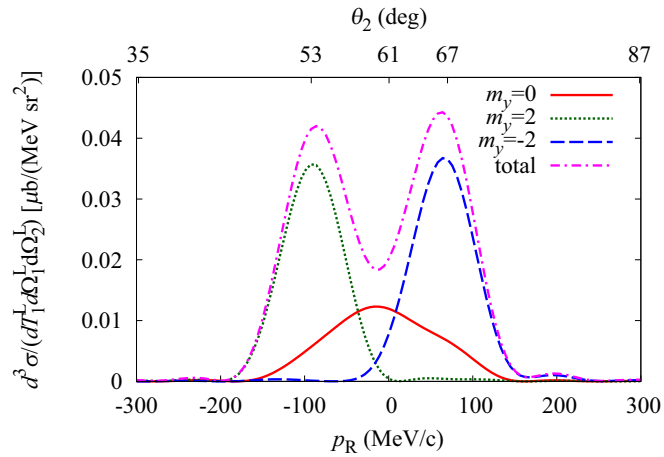

FIG. 2. TDX$_{m_y}$ of ^{120}Sn$(p, p\alpha)\,^{116}$Cd$_{2+}$ at 392 MeV as a function of the recoil momentum. The solid, dotted, and dashed lines represent the components for $m_y = 0$, 2, and -2, respectively. The dot-dashed line shows the sum of all the components.

It is clearly seen that $m_y = 2$ and $m_y = -2$ components are well selected by the kinematics. This is explained as follows. Considering the quasifree knockout reaction, momentum $\boldsymbol{K}_\alpha^{\rm L}$ of b (the bound α particle in A) has an opposite momentum to $\boldsymbol{K}_{\rm B}^{\rm L}$, since the target is at rest in the laboratory frame. Thus, depending on m_y, the position of b to be knocked out can be specified. This implies that b moves to the left (the $-z$ direction) when $p_{\rm R}$ is positive as shown in Fig. 3.

Considering the kinematics that α is emitted to $\theta_2^{\rm L} = 66.5°$ and $\phi_2^{\rm L} = 180°$, the $m_y = 2$ component in Fig. 3 cannot be knocked out because of the short mean-free path of the α particle, which is described by the absorption of the α-^{116}Cd optical potential in the present framework. On the other hand, the $m_y = -2$ component is almost free from the absorption. Therefore the total TDX is dominated by the $m_y = -2$ component when $p_{\rm R}$ is positive. Similarly, when $p_{\rm R}$ is negative, the $m_y = 2$ component becomes dominant. This mechanism has similarities and differences to the Maris effect [35–38] in the nucleon knockout reactions. As for similarities, a classical picture of the orbital motion of the bound particle works to

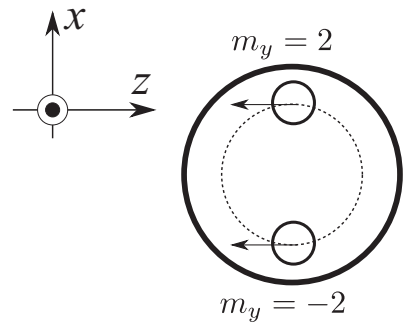

FIG. 3. Classical explanation of the α motion inside the target when $p_{\rm R}$ is positive. In this case, $\boldsymbol{K}_\alpha^{\rm L}$ is parallel to the $-z$ direction. Because the α particle with $m_y = 2$ (-2) revolves counterclockwise (clockwise), its position is specified as in the figure.

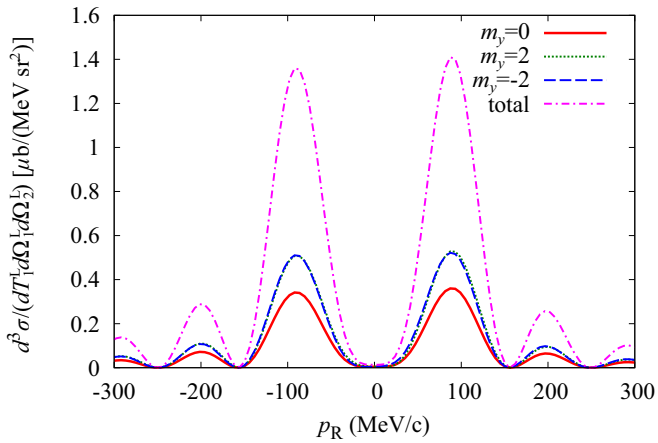

FIG. 4. The same as Fig. 2 but with the plane-wave limit.

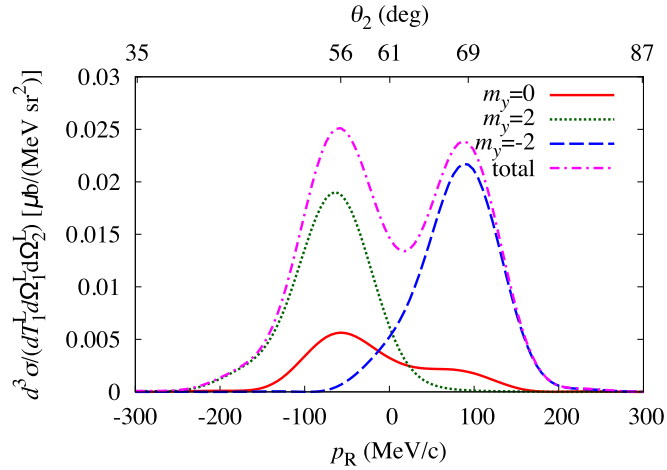

FIG. 5. The Same as Fig. 2 but with microscopic optical potentials.

explain the phenomena. In both the (p, pN) and the $(p, p\alpha)$ cases, the reaction position is restricted to only two positions once the momentum of the bound particle, that is, $\boldsymbol{K}_\alpha^{\rm L}$ in the present study, is given. In addition, the strong absorption effect excludes the contribution from the far side of the two reaction positions with respect to the emitted α direction. Regarding differences, in the Maris effect for (p, pN), the energy of one emitted nucleon is low and that of the other is high, and the former is absorbed. In contrast, in $(p, p\alpha)$, the RPS is realized by the strong absorption, that is, the short mean-free path, of the α particle compared to that of a nucleon. Another typical difference is that in the vector analyzing power of (p, pN), the Maris effect distinguishes the $j_>$ and $j_<$ orbitals for a given angular momentum l by utilizing the strong spin correlation of the NN system. On the other hand, in $(p, p\alpha)$, the present mechanism discriminates m_y and therefore the spin third component of the residue only by the kinematical condition. There is no need for a polarized beam because the transition involves the spinless α particle and the reaction is independent of the spin degrees of freedom.

It should be noted that the $\mathrm{TDX}_{m_y=\pm1}$ vanishes because the integrand in Eq. (1) is antisymmetric with respect to the z-x plane if $l-m$ is odd. This property originates from that of Y_{lm_y}; the remaining part of the integrand in Eq. (1) is symmetric with respect to the z-x plane because the kinematics are taken in coplanar on that plane. Figure 4 shows the same result as in Fig. 2 but with the plane-wave limit. The selectivity found in the DWIA calculation completely disappears and this result clearly shows that the m_y selection is achieved by the absorption effect on the α particle.

Figure 5 displays the results shown in Fig. 2 but calculated with microscopic optical potentials.

As seen, the absolute values of each component of the TDX and its peak positions are changed from those in Fig. 2. For the $m_y = 0$ component, a difference in the shape is also observed. Nevertheless, the dominance of the $m_y = 2$ (-2) component around the peak with negative (positive) $p_{\rm R}$ is found to be robust. For more quantitative discussion, a direct comparison between the results with DWIA and experimental data will be necessary. Investigation of the role of higher-order processes that are not included in DWIA will also be very important. For this purpose, a reaction model (theory) that is applicable to the TDX calculation in complete kinematics, e.g., the FAGS theory, will be needed.

We also calculate the $^{20}\mathrm{Ne}(p, p\alpha)\,^{16}\mathrm{O}_{2^+}$ cross section at 392 MeV. The recoilless condition is realized when $T_1^{\rm L} = 341$ MeV, $\theta_1^{\rm L} = 35^\circ$, $\phi_1^{\rm L} = 0^\circ$, $\theta_2^{\rm L} = 65^\circ$, and $\phi_2^{\rm L} = 180^\circ$. One sees that the shape of the $m_y = 0$ component (solid line) considerably differs from that in Fig. 2 and is similar to what we expect in the PW limit. Thus, this result implies that the distortion effect is weak compared to the $^{120}\mathrm{Sn}(p, p\alpha)\,^{116}\mathrm{Cd}_{2^+}$ case. Nevertheless, the m_y selection still appears in Fig. 6, which will indicate that the nuclear absorption plays a role also in the $^{20}\mathrm{Ne}(p, p\alpha)\,^{16}\mathrm{O}_{2^+}$ case. These results strongly suggest that the effective polarization by the $(p, p\alpha)$ reaction is universal from light to heavy nuclei.

IV. SUMMARY

We have demonstrated that an effective polarization of the residual nucleus is realized in the $^{120}\mathrm{Sn}(p, p\alpha)\,^{116}\mathrm{Cd}_{2^+}$

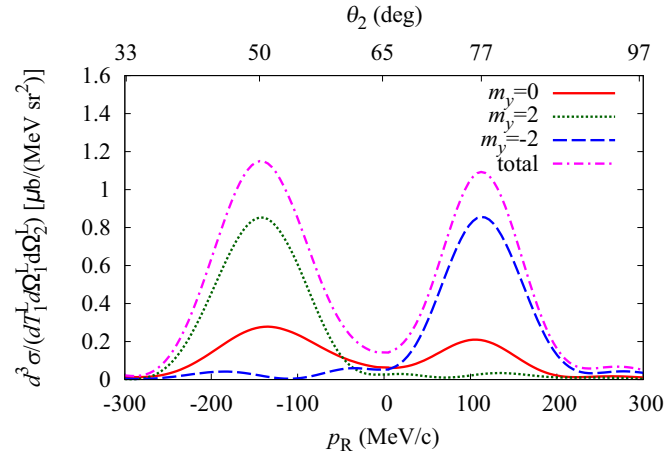

FIG. 6. TDX_{m_y} of $^{20}\mathrm{Ne}(p, p\alpha)\,^{16}\mathrm{O}_{2^+}$ at 392 MeV as a function of the recoil momentum. The same manner as Fig. 2.

and ^{20}Ne$(p, p\alpha)^{16}O_{2^+}$ reaction at 392 MeV. The mechanism of this effective polarization is similar to that of the Maris effect but as a distinct feature, the effective polarization in the $(p, p\alpha)$ processes has nothing to do with the spin degrees of freedom of the reacting particles. In other words, by just measuring the TDX with slightly varying kinematics, a polarized residual nucleus, ^{116}Cd in the 2_1^+ state in this case, can be extracted. This scenario is considered to be the same as for the residue in other spin states. This may be a useful polarization technique based on a kinematically complete direct reaction in both normal and inverse kinematics.

ACKNOWLEDGMENTS

We thank T. Uesaka for fruitful discussions. This work is supported in part by Grants-in-Aid for Scientific Research from the JSPS (Grants No. JP20K14475, No. JP21H00125, and No. JP21H04975) and by JST SPRING, Grant No. JPMJSP2138.

[1] G. Jacob and T. A. J. Maris, Quasi-free scattering and nuclear structure, Rev. Mod. Phys. **38**, 121 (1966).

[2] G. Jacob and T. A. J. Maris, Quasi-free scattering and nuclear structure. ii., Rev. Mod. Phys. **45**, 6 (1973).

[3] T. Wakasa, K. Ogata, and T. Noro, Proton-induced knockout reactions with polarized and unpolarized beams, Prog. Part. Nucl. Phys. **96**, 32 (2017).

[4] L. Olivier, S. Franchoo, M. Niikura, Z. Vajta, D. Sohler, P. Doornenbal, A. Obertelli, Y. Tsunoda, T. Otsuka, G. Authelet, H. Baba, D. Calvet, F. Chateau, A. Corsi, A. Delbart, J. M. Gheller, A. Gillibert, T. Isobe, V. Lapoux, M. Matsushita *et al.*, Persistence of the Z = 28 Shell Gap Around ^{78}Ni: First Spectroscopy of ^{79}Cu, Phys. Rev. Lett. **119**, 192501 (2017).

[5] S. Kawase, T. Uesaka, T. L. Tang, D. Beaumel, M. Dozono, T. Fukunaga, T. Fujii, N. Fukuda, A. Galindo-Uribarri, S. Hwang, N. Inabe, T. Kawabata, T. Kawahara, W. Kim, K. Kisamori, M. Kobayashi, T. Kubo, Y. Kubota, K. Kusaka, C. Lee *et al.*, Exclusive quasi-free proton knockout from oxygen isotopes at intermediate energies, Prog. Theor. Exp. Phys. **2018**, 021D01 (2018).

[6] Z. Elekes, A. Kripkó, D. Sohler, K. Sieja, K. Ogata, K. Yoshida, P. Doornenbal, A. Obertelli, G. Authelet, H. Baba, D. Calvet, F. Château, A. Corsi, A. Delbart, J.-M. Gheller, A. Gillibert, T. Isobe, V. Lapoux, M. Matsushita, S. Momiyama *et al.*, and Z. Xu (SunFlower Collaboration), Nuclear structure of ^{76}Ni from the $(p, 2p)$ reaction, Phys. Rev. C **99**, 014312 (2019).

[7] R. Taniuchi, C. Santamaria, P. Doornenbal, A. Obertelli, K. Yoneda, G. Authelet, H. Baba, D. Calvet, F. Château, A. Corsi, A. Delbart, J.-M. Gheller, A. Gillibert, J. D. Holt, T. Isobe, V. Lapoux, M. Matsushita, J. Menéndez, S. Momiyama, T. Motobayashi *et al.*, ^{78}Ni revealed as a doubly magic stronghold against nuclear deformation, Nature (London) **569**, 53 (2019).

[8] S. Chen, J. Lee, P. Doornenbal, A. Obertelli, C. Barbieri, Y. Chazono, P. Navrátil, K. Ogata, T. Otsuka, F. Raimondi, V. Somà, Y. Utsuno, K. Yoshida, H. Baba, F. Browne, D. Calvet, F. Château, N. Chiga, A. Corsi, M. L. Cortés *et al.*, Quasifree Neutron Knockout from ^{54}Ca Corroborates Arising $N = 34$ Neutron Magic Number, Phys. Rev. Lett. **123**, 142501 (2019).

[9] M. Cortés, W. Rodriguez, P. Doornenbal, A. Obertelli, J. Holt, S. Lenzi, J. Menéndez, F. Nowacki, K. Ogata, A. Poves, T. Rodríguez, A. Schwenk, J. Simonis, S. Stroberg, K. Yoshida, L. Achouri, H. Baba, F. Browne, D. Calvet, F. Château *et al.*, Shell evolution of N = 40 isotones towards ^{60}Ca: First spectroscopy of ^{62}Ti, Phys. Lett. B **800**, 135071 (2020).

[10] Y. Sun, A. Obertelli, P. Doornenbal, C. Barbieri, Y. Chazono, T. Duguet, H. Liu, P. Navrátil, F. Nowacki, K. Ogata, T. Otsuka, F. Raimondi, V. Somà, Y. Utsuno, K. Yoshida, N. Achouri, H. Baba, F. Browne, D. Calvet, F. Château *et al.*, Restoration of the natural $E(1/2_1^+)$ - $E(3/2_1^+)$ energy splitting in odd-K isotopes towards $N = 40$, Phys. Lett. B **802**, 135215 (2020).

[11] T. Lokotko, S. Leblond, J. Lee, P. Doornenbal, A. Obertelli, A. Poves, F. Nowacki, K. Ogata, K. Yoshida, G. Authelet, H. Baba, D. Calvet, F. Château, S. Chen, A. Corsi, A. Delbart, J.-M. Gheller, A. Gillibert, T. Isobe, V. Lapoux *et al.*, Shell structure of the neutron-rich isotopes ^{69,71,73}Co, Phys. Rev. C **101**, 034314 (2020).

[12] T. L. Tang, T. Uesaka, S. Kawase, D. Beaumel, M. Dozono, T. Fujii, N. Fukuda, T. Fukunaga, A. Galindo-Uribarri, S. H. Hwang, N. Inabe, D. Kameda, T. Kawahara, W. Kim, K. Kisamori, M. Kobayashi, T. Kubo, Y. Kubota, K. Kusaka, C. S. Lee *et al.*, How Different is the Core of ^{25}F from $^{24}O_{g.s.}$? Phys. Rev. Lett. **124**, 212502 (2020).

[13] Y. Kubota, A. Corsi, G. Authelet, H. Baba, C. Caesar, D. Calvet, A. Delbart, M. Dozono, J. Feng, F. Flavigny, J.-M. Gheller, J. Gibelin, A. Giganon, A. Gillibert, K. Hasegawa, T. Isobe, Y. Kanaya, S. Kawakami, D. Kim, Y. Kikuchi *et al.*, Surface Localization of the Dineutron in ^{11}Li, Phys. Rev. Lett. **125**, 252501 (2020).

[14] M. L. Cortés, W. Rodriguez, P. Doornenbal, A. Obertelli, J. D. Holt, J. Menéndez, K. Ogata, A. Schwenk, N. Shimizu, J. Simonis, Y. Utsuno, K. Yoshida, L. Achouri, H. Baba, F. Browne, D. Calvet, F. Château, S. Chen, N. Chiga, A. Corsi *et al.*, $N = 32$ shell closure below calcium: Low-lying structure of ^{50}Ar, Phys. Rev. C **102**, 064320 (2020).

[15] Z. H. Yang *et al.*, Quasifree Neutron Knockout Reaction Reveals a Small s-Orbital Component in the Borromean Nucleus ^{17}B, Phys. Rev. Lett. **126**, 082501 (2021).

[16] M. Juhász, Z. Elekes, D. Sohler, Y. Utsuno, K. Yoshida, T. Otsuka, K. Ogata, P. Doornenbal, A. Obertelli, H. Baba, F. Browne, D. Calvet, F. Château, S. Chen, N. Chiga, A. Corsi, M. Cortés, A. Delbart, J.-M. Gheller, A. Giganon *et al.*, First spectroscopic study of ^{51}Ar by the $(p, 2p)$ reaction, Phys. Lett. B **814**, 136108 (2021).

[17] M. M. Juhász, Z. Elekes, D. Sohler, K. Sieja, K. Yoshida, K. Ogata, P. Doornenbal, A. Obertelli, H. Baba, F. Browne, D. Calvet, F. Château, S. Chen, N. Chiga, A. Corsi, M. L. Cortés, A. Delbart, J.-M. Gheller, A. Giganon, A. Gillibert *et al.*, First spectroscopic study of ^{63}V at the $n = 40$ island of inversion, Phys. Rev. C **103**, 064308 (2021).

[18] F. Browne, S. Chen, P. Doornenbal, A. Obertelli, K. Ogata, Y. Utsuno, K. Yoshida, N. L. Achouri, H. Baba, D. Calvet, F. Château, N. Chiga, A. Corsi, M. L. Cortés, A. Delbart, J.-M. Gheller, A. Giganon, A. Gillibert, C. Hilaire, T. Isobe *et al.*, Pairing Forces Govern Population of Doubly Magic

^{54}Ca from Direct Reactions, Phys. Rev. Lett. **126**, 252501 (2021).

[19] B. D. Linh, A. Corsi, A. Gillibert, A. Obertelli, P. Doornenbal, C. Barbieri, S. Chen, L. X. Chung, T. Duguet, M. Gómez-Ramos, J. D. Holt, A. Moro, P. Navrátil, K. Ogata, N. T. T. Phuc, N. Shimizu, V. Somà, Y. Utsuno, N. L. Achouri, H. Baba *et al.*, Investigation of the ground-state spin inversion in the neutron-rich ^{47,49}Cl isotopes, Phys. Rev. C **104**, 044331 (2021).

[20] A. M. Moro, Three-body model for the analysis of quasifree scattering reactions in inverse kinematics, Phys. Rev. C **92**, 044605 (2015).

[21] M. Gómez-Ramos and A. Moro, Binding-energy independence of reduced spectroscopic strengths derived from $(p, 2p)$ and (p, pn) reactions with nitrogen and oxygen isotopes, Phys. Lett. B **785**, 511 (2018).

[22] T. Aumann, C. A. Bertulani, and J. Ryckebusch, Quasifree $(p, 2p)$ and (p, pn) reactions with unstable nuclei, Phys. Rev. C **88**, 064610 (2013).

[23] E. Cravo, R. Crespo, and A. Deltuva, Distortion effects on the neutron knockout from exotic nuclei in the collision with a proton target, Phys. Rev. C **93**, 054612 (2016).

[24] R. Crespo, E. Cravo, and A. Deltuva, Three-body calculations for (p, pn) reactions: Kinematically inclusive, semi-inclusive, and fully exclusive cross sections, Phys. Rev. C **99**, 054622 (2019).

[25] A. Mecca, E. Cravo, A. Deltuva, R. Crespo, A. Cowley, A. Arriaga, R. Wiringa, and T. Noro, Interplay of dynamical and structure effects in the observables for 12c(p,2p) near 400 mev with polarized and unpolarized beams, Phys. Lett. B **798**, 134989 (2019).

[26] K. Yoshida, M. Gómez-Ramos, K. Ogata, and A. M. Moro, Benchmarking theoretical formalisms for (p, pn) reactions: The ^{15}C$(p, pn)^{14}$C case, Phys. Rev. C **97**, 024608 (2018).

[27] M. Gómez-Ramos, A. Deltuva, and A. M. Moro, Benchmarking faddeev and transfer-to-the-continuum calculations for (p, pn) reactions, Phys. Rev. C **102**, 064613 (2020).

[28] J. Tanaka, Z. Yang, S. Typel, S. Adachi, S. Bai, P. van Beek, D. Beaumel, Y. Fujikawa, J. Han, S. Heil, S. Huang, A. Inoue, Y. Jiang, M. Knösel, N. Kobayashi, Y. Kubota, W. Liu, J. Lou, Y. Maeda, Y. Matsuda *et al.*, Formation of α clusters in dilute neutron-rich matter, Science **371**, 260 (2021).

[29] S. Typel, Neutron skin thickness of heavy nuclei with α-particle correlations and the slope of the nuclear symmetry energy, Phys. Rev. C **89**, 064321 (2014).

[30] T. Aumann, C. Barbieri, D. Bazin, C. A. Bertulani, A. Bonaccorso, W. H. Dickhoff, A. Gade, M. Gómez-Ramos, B. P. Kay, A. M. Moro, T. Nakamura, A. Obertelli, K. Ogata, S. Paschalis, and T. Uesaka, Quenching of single-particle strength from direct reactions with stable and rare-isotope beams, Prog. Part. Nucl. Phys. **118**, 103847 (2021).

[31] J. Casal and M. Gómez-Ramos, Opening angle and dineutron correlations in knockout reactions with borromean two-neutron halo nuclei, Phys. Rev. C **104**, 024618 (2021).

[32] M. Yamagami, Momentum-space structure of dineutrons in borromean nuclei, Phys. Rev. C **106**, 044316 (2022).

[33] K. Yoshida, K. Minomo, and K. Ogata, Investigating α clustering on the surface of ^{120}Sn via the $(p, p\alpha)$ reaction, and the validity of the factorization approximation, Phys. Rev. C **94**, 044604 (2016).

[34] K. Yoshida, K. Ogata, and Y. Kanada-En'yo, Investigation of α clustering with knockout reactions, Phys. Rev. C **98**, 024614 (2018).

[35] T. Maris, Quasi-free nucleon-nucleon scattering, Nucl. Phys. **9**, 577 (1958).

[36] G. Jacob, T. A. Maris, C. Schneider, and M. Teodoro, Quasi-free scattering with polarized protons, Nucl. Phys. A **257**, 517 (1976).

[37] T. Maris, M. Teodoro, and C. Vasconcellos, Nuclear information from quasi-free scattering with polarized protons, Nucl. Phys. A **322**, 461 (1979).

[38] G. Krein, T. A. J. Maris, B. B. Rodrigues, and E. A. Veit, Medium effects on spin observables of proton knockout reactions, Phys. Rev. C **51**, 2646 (1995).

[39] C. W. Wang, P. G. Roos, N. S. Chant, G. Ciangaru, F. Khazaie, D. J. Mack, A. Nadasen, S. J. Mills, R. E. Warner, E. Norbeck, F. D. Becchetti, J. W. Janecke, and P. M. Lister, ^{9}Be$(p, p\alpha)^{5}$He cluster knockout reaction with 150 MeV polarized protons, Phys. Rev. C **31**, 1662 (1985).

[40] R. Neveling, A. A. Cowley, Z. Buthelezi, S. V. Förtsch, H. Fujita, G. C. Hillhouse, J. J. Lawrie, G. F. Steyn, F. D. Smit, S. M. Wyngaardt, N. T. Botha, L. Mudau, and S. S. Ntshangase, Analyzing power of the ^{40}Ca$(\vec{p}, p\alpha)$ reaction at 100 MeV, Phys. Rev. C **77**, 037601 (2008).

[41] A. A. Cowley, J. Mabiala, E. Z. Buthelezi, S. V. Förtsch, R. Neveling, F. D. Smit, G. F. Steyn, and J. J. van Zyl, Analyzing power distribution in the ^{12}C$(p, p\alpha)^{8}$Be(g.s.) reaction at an incident energy of 100 MeV, Europhys. Lett. **85**, 22001 (2009).

[42] J. Mabiala, A. A. Cowley, S. V. Förtsch, E. Z. Buthelezi, R. Neveling, F. D. Smit, G. F. Steyn, and J. J. Van Zyl, Analyzing power and cross section distributions of the ^{12}C$(p, p\alpha)^{8}$Be cluster knockout reaction at an incident energy of 100 MeV, Phys. Rev. C **79**, 054612 (2009).

[43] A. A. Cowley, Sensitivity of analyzing power to distorting potentials in the quasifree reaction ^{40}Ca$(p, p\alpha)^{36}$Ar at 100 MeV incident energy: Comparison with ^{9}Be and ^{12}C targets, Phys. Rev. C **103**, 034622 (2021).

[44] P. Hansen and J. Tostevin, Direct reactions with exotic nuclei, Annu. Rev. Nucl. Part. Sci. **53**, 219 (2003).

[45] M. Lyu, K. Yoshida, Y. Kanada-En'yo, and K. Ogata, Manifestation of α clustering in ^{10}Be via α-knockout reaction, Phys. Rev. C **97**, 044612 (2018).

[46] M. Lyu, K. Yoshida, Y. Kanada-En'yo, and K. Ogata, Direct probing of the cluster structure in ^{12}Be via the α-knockout reaction, Phys. Rev. C **99**, 064610 (2019).

[47] K. Yoshida, Y. Chiba, M. Kimura, Y. Taniguchi, Y. Kanada-En'yo, and K. Ogata, Quantitative description of the ^{20}Ne$(p, p\alpha)^{16}$O reaction as a means of probing the surface α amplitude, Phys. Rev. C **100**, 044601 (2019).

[48] Y. Taniguchi, K. Yoshida, Y. Chiba, Y. Kanada-En'yo, M. Kimura, and K. Ogata, Unexpectedly enhanced α-particle preformation in ^{48}Ti probed by the $(p, p\alpha)$ reaction, Phys. Rev. C **103**, L031305 (2021).

[49] S. E. Darden, in *Proceedings of the Third International Symposium on Polarization Phenomena in Nuclear Reactions*, edited by H. Barschall and W. Haeberli (University of Wisconsin Press, Madison, 1971), p. 39.

[50] N. S. Chant and P. G. Roos, Distorted-wave impulse-approximation calculations for quasifree cluster knockout reactions, Phys. Rev. C **15**, 57 (1977).

[51] N. S. Chant and P. G. Roos, Spin orbit effects in quasifree knockout reactions, Phys. Rev. C **27**, 1060 (1983).
[52] S. Saito, Interaction between clusters and Pauli principle, Prog. Theor. Phys. **41**, 705 (1969).
[53] M. Toyokawa, K. Minomo, and M. Yahiro, Mass-number and isotope dependence of local microscopic optical potentials for polarized proton scattering, Phys. Rev. C **88**, 054602 (2013).
[54] K. Amos, P. J. Dortmans, H. V. von Geramb, S. Karataglidis, and J. Raynal, Nucleon-nucleus scattering: A microscopic nonrelativistic approach, Adv. Nucl. Phys. **25**, 276 (2000).
[55] H. De Vries, C. De Jager, and C. De Vries, Nuclear charge-density-distribution parameters from elastic electron scattering, At. Data Nucl. Data Tables **36**, 495 (1987).
[56] R. Singhal, M. Macauley, and P. De Witt Huberts, Folding of proton size in nuclear structure calculations, Nucl. Instrum. Meth. **148**, 113 (1978).
[57] A. Koning and J. Delaroche, Local and global nucleon optical models from 1 keV to 200 MeV, Nucl. Phys. A **713**, 231 (2003).
[58] V. Avrigeanu, P. E. Hodgson, and M. Avrigeanu, Global optical potentials for emitted alpha particles, Phys. Rev. C **49**, 2136 (1994).
[59] A. Bohr and B. Mottelson, *Nuclear Structure* (W. A. Benjamin, San Francisco, 1969).
[60] K. Egashira, K. Minomo, M. Toyokawa, T. Matsumoto, and M. Yahiro, Microscopic optical potentials for ^{4}He scattering, Phys. Rev. C **89**, 064611 (2014).